DOI:10.1190/INT-2019-0307.1

Experience on controlled-source electromagnetic performance for exploration in Norway

Lodve Berre[1], Jan Petter Morten[1], Graeme Baillie[1], and Elias Nerland[1]

Abstract

We have analyzed the predictive performance of the controlled-source electromagnetic (CSEM) method using a large statistical database. The prediction strength is quantified by comparing the CSEM interpretation to exploration drilling results for more than 100 wells in Norway. The comparison has been done by correlating inversion results for all of the surveys covering these wells with the well outcome, using a statistically driven anomaly detection workflow to avoid confirmation bias. The comparison is summarized by classifying the interpretations as true positives, true negatives, false positives, or false negatives. We find that the CSEM interpretation correctly identified the true negative and positive cases for 79% of the analyzed wells. We further evaluate how integrated interpretation can provide more detailed predictions. This includes taking the sensitivity to the target into account as well as integrating seismic data and rock-physics parameters with the CSEM data to quantify the potential volumes in place. In some cases, we also determine that the derived parameters are not compatible with hydrocarbon models, and prospects must be downgraded despite having clear CSEM anomalies associated with them. In addition to the statistics, our results are supported by several case examples.

Introduction

Seismic data are the cornerstone of exploration and have been the driver for the development of Europe's marine oil and gas activities. This fact motivates the persistent interest and investment in seismic acquisition and seismic imaging technology development. However, investigations of current discovery and resource replacement rates show that exploration drilling technical and commercial success rates are declining (Westwood Global Energy Group, 2018). This is the background for a renewed industry interest in multiphysics approaches and integrated interpretation. The controlled-source electromagnetic (CSEM) method is inherently sensitive to the volume of reservoir hydrocarbon saturation. Therefore, it should prove an ideal tool to supplement seismic for increasing commercial success rates because CSEM will not be sensitive to the small volumes discovered by exploration wells that are merely considered technically successful.

In this paper, we investigate and quantify the predictive performance of CSEM. We also describe and demonstrate with application examples how integrated interpretation workflows improve predictions. Our study is based on the large CSEM database resulting from close to 1000 node-based surveys acquired by EMGS since 2002. The database includes measurements from more than 60,000 receiver drops and source towing corresponding to a distance exceeding 250,000 km (6.2 times around the equator). The survey coverage includes all of the world's most prolific marine basins. From this large global database, several hundred coinciding wells can be used to calibrate the CSEM prediction against the drilling results. In Norway alone (Figure 1), we have access to more than 150 exploration wells as calibration points for multiclient data. We will use statistics from this database to determine the prediction strength and the potential of CSEM to impact discovery rates.

We also include old legacy data in our study because we want to determine if the advances in imaging technology have changed the interpretation from the time of acquisition. One case considered is the legacy 2D survey from the Grane field. The CSEM survey was acquired in 2003. Due to seismic impedance properties, the Grane reservoir sands are not easily imaged using conventional streamer seismic (Figure 2a). The target zone has a "transparent" signature, and the exploration wells were drilled based on thickness variations in the target zone isochore without definite direct hydrocarbon indicator (DHI) support. Though the shale-sand contrast is improved on 4C seismic to the degree that the Heimdal sands can more easily be mapped (Figure 2b), 4C seismic is rarely available for exploration drilling decisions. As shown in Figure 2c, the Grane

[1]EMGS ASA, Trondheim 7440, Norway. E-mail: lodve@berre.no (corresponding author); jan.petter.morten@inphase.no; gbaillie@westnet.com.au; enerland@emgs.com.

Manuscript received by the Editor 3 January 2020; revised manuscript received 18 May 2020; published ahead of production 19 June 2020; published online 31 August 2020. This paper appears in *Interpretation*, Vol. 8, No. 4 (November 2020); p. SQ25–SQ37, 17 FIGS.

http://dx.doi.org/10.1190/INT-2019-0307.1.

field could not be seen on the CSEM attribute analysis available at the time of the acquisition. However, the result from reprocessing and inversion of the original CSEM survey data using state-of-the-art methods, shown in Figure 2d, reveals a clear resistivity anomaly associated with the Grane field.

We propose to analyze the performance of a geophysical method such as CSEM according to three main categories: first, the accuracy and reliability of the measured data, second the subsurface imaging, and third the *interpretation* of the imaging results. The measured data accuracy can be quantified by detailed hardware testing and calibration and the impact on the processed data including all of the operational factors calculated using error propagation (Mittet and Morten, 2012). For CSEM acquisition, the measurement accuracy contribution toward the final results' reliability is a cost issue and the impact can be quantified. Large improvements in signal-to-noise ratios (S/Ns) have recently been achieved by the introduction of new and more powerful sources (Nguyen et al., 2016). The S/N improvement effect is shown in Figure 3. In this figure, we show two inversion results for the Norwegian Sea Njord field. In one case, the input data were acquired by operating the source at high power 7200 A (right), and in the other case the current during transmission was reduced to 1200 A (left), which is representative of previous-generation source equipment. The increased current output has a significant effect in enhancing deep target imaging. This is in line with the sensitivity assessment for the two results, shown as a function of the resistor area and anomalous transverse resistance (ATR) (Mittet and Morten, 2013) in the figure insets. We defined the subsurface imaging technology as the second category of factors that affect the CSEM performance. The exploration application of CSEM has driven the development of large-scale full-waveform inversion codes (Ziolkowski and Slob, 2019) supporting anisotropic 3D modeling and higher order optimization strategies. As an example, the impact of the introduction of 3D Gauss-Newton inversion was documented by Nguyen et al. (2017). It is currently possible to routinely achieve a good data fit with 3D inversion incorporating a realistic medium representation. Therefore, one can argue that the largest improvement potential currently lies in applying a robust interpretation workflow. Such a workflow should include sensitivity studies, synthetic scenario testing, and anomaly identification and should also consider rock-physics and reservoir models in the integration of CSEM, seismic, and well data. Integration of data involves correlation of seismic structures, geometries, DHIs, prospect outlines, and reservoir models. When integrating CSEM data, it is important to account for possible interpretation pitfalls such as lack of target sensitivity and the risk of other resistive lithologies. In this paper, we determine the performance of CSEM considering uncertainty in the imaging interpretation.

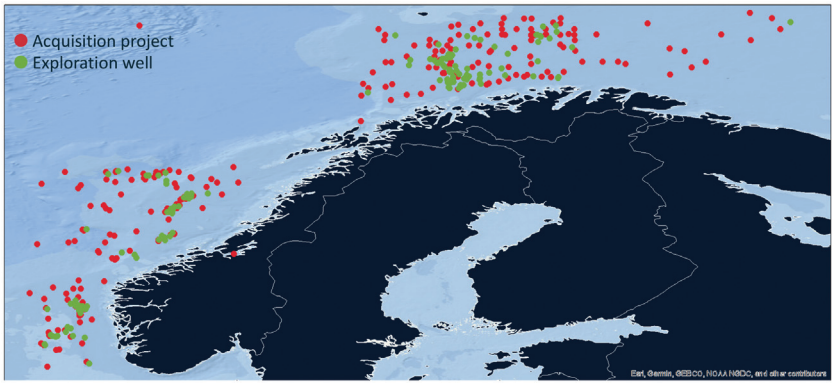

Figure 1. Exploration wells covered by EMGS's Norwegian CSEM MC coverage per 2019. The red dots show the approximate locations for CSEM surveys, and the green dots show exploration well locations where the drilling results can be used to evaluate CSEM-based predictions.

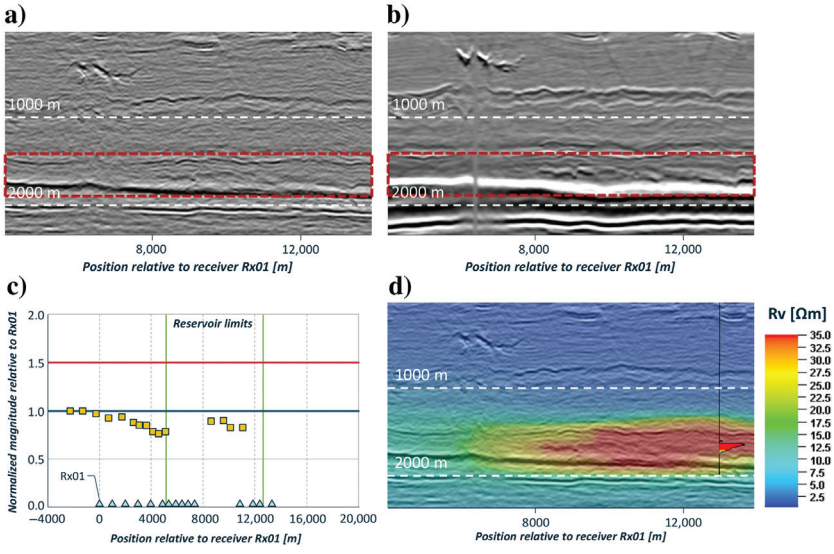

Figure 2. (a) Streamer seismic over the Grane field. The reservoir section is very transparent because the acoustic impedance contrast between the shale and the reservoir sands is small. (b) 4C seismic over the Grane field. The PS-seismic improves the shale-sand contrast, and the Heimdal sands are more easily mapped. (c) 2003 magnitude versus offset interpretation of CSEM over the Grane field. The field outline is between the purple lines. (d) Recent inversion of the 2003 CSEM data overlaid on the streamer seismic. The CSEM anomaly corresponds very well to the reservoir section laterally and in depth.

DOI:10.1190/INT-2019-0307.1

CSEM to well results correlation workflow

We will now describe the results from comparing the CSEM prediction against the drilling results for the surveys in Norway. In our statistical analysis, where we correlate CSEM results to well outcomes, we use the following workflow for each case:

a) Assess inversion quality — has the inversion been able to fit the data within the measurement uncertainty?
b) Assess vertical section through well (s) — can a clear correlation to well results be seen in the vertical section?
c) Assess average resistivity through the target interval, and use histogram-based anomaly detection.

The steps in this workflow are illustrated in Figure 4. Data misfit maps are a by-product from inversion and can readily assess whether the result is suitable for further analysis (step [a]). In step (b), we show how resistivity well logs can be covisualized with the inversion results allowing us to qualitatively understand the correlation between CSEM data inverted resistivities and log values. In step (c), we map the target-level resistivity laterally and inspect the resulting resistivity histogram to define the outline of a resistor (Barker and Baltar, 2016). This gives further qualification of the well result and resistor correlation, which is often important to assess because exploration wells are typically located close to the expected hydrocarbon reservoir edge and we must assess whether the well penetrates inside or outside the predicted saturated reservoir lateral extension.

If an anomaly can be identified in the vertical section and the histogram-based map for the target interval average, we classify the result as a CSEM positive. If an anomaly cannot be identified, we classify the result as a CSEM negative. We then correlate the CSEM results to the well results as published by the Norwegian Petroleum Directorate (NPD), where shows and dry wells are classified as negatives, and any discovery is classified as a positive regardless of the volumes and likely commerciality.

Database and selection criteria

For 3D surveys, we have included all of the exploration wells within the receiver coverage, whereas for 2D surveys, we have included exploration wells offset up to 1,000 m from the receiver line. We have also chosen to include wells that were drilled prior to and after the CSEM data was acquired because many calibration

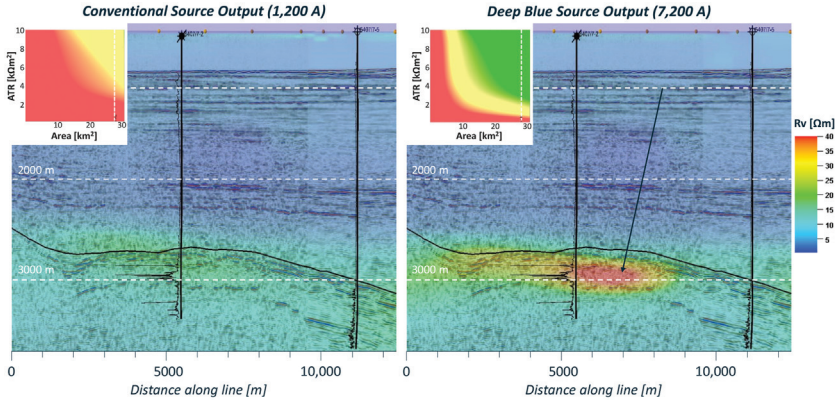

Figure 3. Comparison of the inversion results (with seismic overlay) from the same line over the Njord field with source outputs of 1200 A (left) and 7000 A (right). The increased source power enhances the S/N and allows reliable imaging at depth. This has a significant effect on the result for the Njord field at almost 3 km depth. Only when using the 7000 A output is a clear resistive anomaly imaged at the hydrocarbon reservoir location. The top-left insets show the result of a data sensitivity analysis with the color coding: green, good sensitivity; yellow, moderate sensitivity; and red, low sensitivity. The axes are the resistor area and ATR. The analysis shows that good sensitivity requires the enhanced measurement accuracy provided by the high current output, in agreement with the actual inversion results.

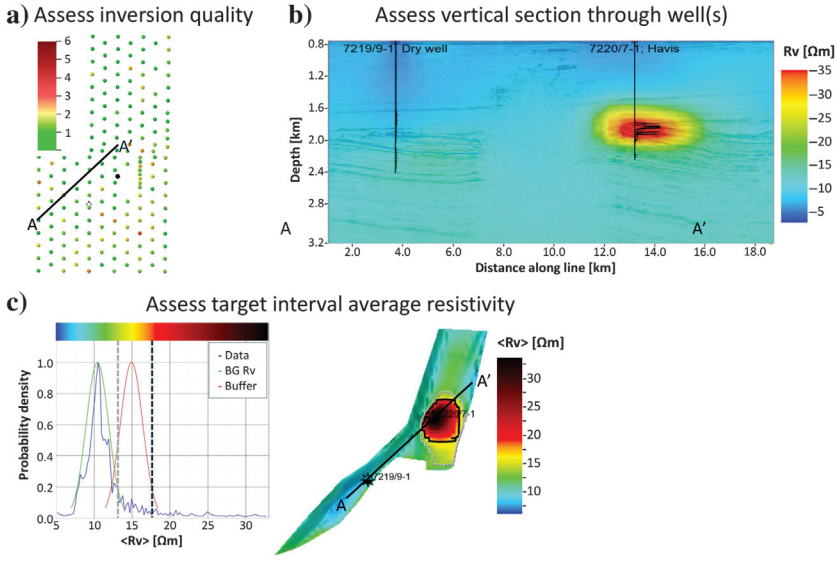

Figure 4. (a) Root-mean-square (rms) misfit for each receiver represented as colored circles on the survey layout grid. The scale is in units of estimated sample standard deviation, where green shows a misfit of less than 1 (a good fit) and red shows a misfit larger than 3 (a poor fit). In this example, most receivers have a good misfit but the receivers marked by red should be investigated to understand the origin of the higher misfit. (b) Vertical section used for step b in evaluation of the inversion result for the 7220/7-1 Havis discovery and the 7219/9-1 dry well. (c) Average resistivity (<Rv>) histogram-based anomaly evaluation and map for the target interval, used for step c for the 7220/7-1 Havis discovery and the 7219/9-1 dry well.

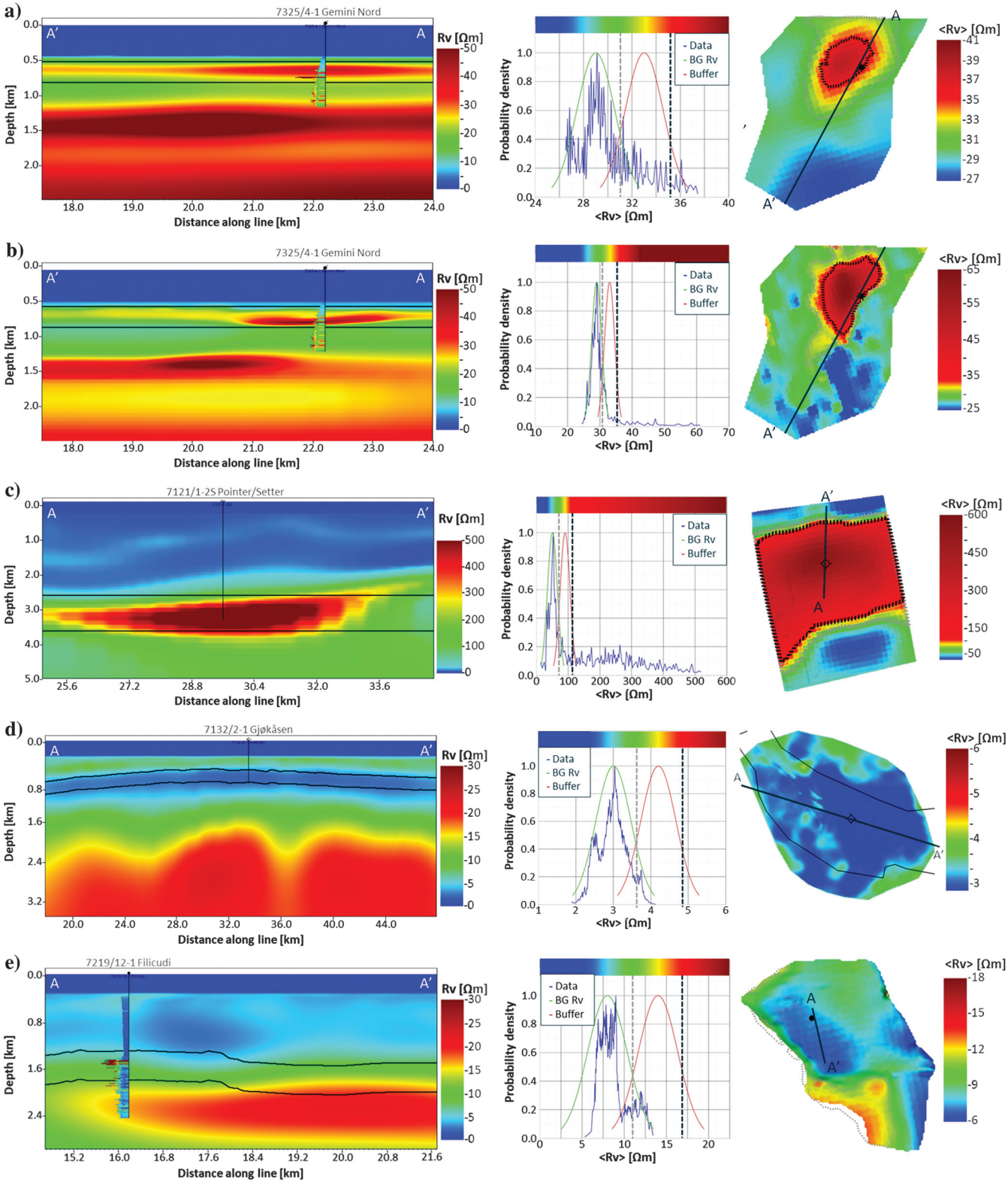

Figure 5. Examples of (a and b) true-positive, (c) false-positive, (d) true-negative, and (e) false-negative cases from the Barents Sea. All average resistivity sections to the right are extracted through the intervals indicated by the black lines in the vertical sections to the left. The histograms in the middle represent the distribution of the average resistivity values. Where horizontal resistivity well logs are available, we have superimposed these on the vertical resistivity from the inversion results for reference using the same color scale.

points were picked to test the limits of the technology and will, as such, provide valuable information. It is, however, important to keep in mind that this first part of this article is a statistical correlation analysis, and not a prospect evaluation study.

CSEM to well results correlation

When presenting the performance statistics, we will first evaluate the CSEM performance as a well prediction tool. This will be based on the published hydrocarbon outcome of the wells by NPD compared to interpretation of the CSEM inversion results without integrated interpretation. To simulate the predrill setting, no a priori information is used during the inversions. Subsequently, we will take a closer look at some of the failures to highlight how an integrated interpretation approach may have helped avoid failure, in addition to looking into how integrated interpretation might bring additional value to the successful cases.

The CSEM performance outcome is classified into four categories by comparing the positive and negative distinctions defined above. The CSEM interpretation failures are either false negatives (hydrocarbon accumulation discovery with no resistive anomaly; see Figure 5e) or false positives (no hydrocarbon accumulation with a resistive anomaly; see Figure 5c). In general, the false-negative category is often caused by a lack of sensitivity due to a small reservoir size or a large burial depth. The false-positive category is often caused by a tight reservoir or presence of other highly resistive lithologies. The categories true positive (Figure 5a and 5b) and true negative (Figure 5d) represent the correct correlation between the well outcome and the CSEM interpretation. These four classifiers provide a prediction strength measure for the CSEM method. Quantification of the CSEM performance can be used to support implementation of CSEM in workflows to upgrade or downgrade a seismic prospect and enable a better understanding of how and when to apply the CSEM method.

We will now describe the examples in Figure 5 with more detail. Figure 5a and 5b shows the results at well 7325/4-1 for the Gemini North prospect. This is a true-positive example from the Barents Sea for a shallow gas discovery. The resistor was first imaged using a coarse-grid (3 km receiver and transmitter line spacing) exploration survey data set, and it was processed using a 3D gradient-based inversion algorithm (Figure 5a). Later, a high-resolution dense-grid (1 km receiver spacing and 0.5 km transmitter line spacing) survey data set was acquired in 2018 for detailed characterization of prospects in this license block. The high-resolution data were processed using a 3D Gauss-Newton inversion algorithm (Figure 5b). Note the increased spatial resolution and ATR recovery from the dense data set. For (a and b), the average resistivity is extracted using the same 300 m thick constant interval at the target level.

Figure 5c shows well 7121/1-25 for the Pointer and Setter prospects in the Barents Sea. This CSEM result represents a false-positive example. The average resistivity map shown is extracted using a 1000 m thick constant interval covering the target levels. A robust, strong resistive anomaly is imaged by the CSEM, but the well did not encounter hydrocarbons but rather a resistive lithology.

Figure 5d shows well 7132/2-1 for the Gjøkåsen prospect in the Barents Sea. This is a true-negative example. The primary target was reservoir sands in the mid to early Jurassic interval (the Stø, Nordmela, Tubåen, and Fruholmen Formations). The predrill volume estimates ranged from 100 to 1000 MMboe, whereas the CSEM results indicated a dry well with no resistive anomaly imaged at the target level. The average resistivity window used to produce the map is a 300 m interval at the mid-Jurassic level (the horizons are courtesy of TGS). The predrill prospect outline is indicated by black lines in the average resistivity map. The well outcome was reported as being dry.

Figure 5e shows the result at the well 7219/12-1 location for the Filicudi prospect. This is an example of a false-negative case from the Barents Sea. The average resistivity displayed to the right is extracted from a 500 m thick interval 250 m above and below the Base Jurassic level (shown in the vertical section to the left). The well encountered oil and gas, and the volume is currently reported as 23 MMboe.

A summary of the statistics from the correlation analysis is shown in Figure 6. The total number of wells included was 104. It is important to note that the results presented in Figure 6 did not include integrated interpretation, and they only refer to the absence or presence of a resistive anomaly in comparison to the well results. No volume limits or sensitivity thresholds have been imposed on the false-negative cases, so these samples will include any volumes of moveable hydrocarbons found, regardless of volume. Where possible, we have used the anomaly-detection workflow described by Barker and Baltar (2016) when defining the resistor extent to avoid confirmation bias. We consider that there is a positive correlation between hydrocarbon accumulations and the CSEM resistive anomaly if the discovery level is within the anomaly in lateral extent and in depth. When the results for one reason or another

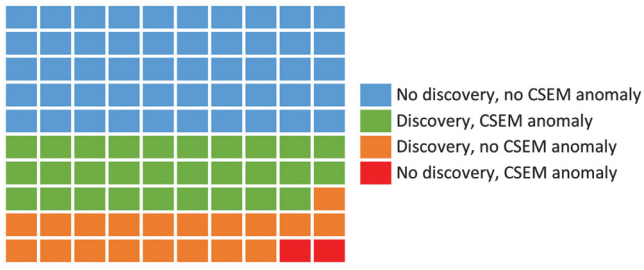

Figure 6. Correlation between well results and CSEM for 104 exploration wells from the Norwegian continental shelf. The sample includes wells from the North, Norwegian, and Barents Seas. Each cell represents 1%.

DOI:10.1190/INT-2019-0307.1

have been deemed ambiguous, we have chosen to take a conservative approach and classify them as either false negatives or false positives.

Even with these very conservative criteria, we see that CSEM predictions are correctly correlated to the actual well results in 79% of the cases for the Norwegian sample. This exceeds the typical wildcat drilling success ratio and implies that CSEM technology can significantly enhance the efficiency of exploration. Furthermore, we will show that the CSEM prediction strength increases dramatically if an integrated interpretation approach is implemented. This is particularly effective for the false-positive cases, where resistive lithologies instead of hydrocarbons were found by exploration drilling.

Integrated interpretation

We will now discuss how integrated interpretation can help to further increase the success rate. Extending the correlation workflow described above, we will also take into account the sensitivity to the target when interpreting the CSEM results. The steps of the assessment workflow described below are illustrated by the examples in Figure 7.

The workflow followed for data going into the integrated interpretation is as follows:

a) Assess the sensitivity to the target — which volumes are likely to be detected for the given setting? This includes assessing the source frequencies used as well as the acquisition geometry. The top left plot in Figure 7 shows the target response normalized to the measurement uncertainty in color scale for the variable target ATR and area. If the calculated sensitivity is good (in green; i.e., the target response exceeds three measurement standard deviations), then the target is expected to be imaged.

b) Assess inversion quality — has the inversion been able to fit the measured data within the measurement uncertainty? This is evaluated by inspecting residual maps that are an additional output from the 3D inversion along with the resistivity model. In case of a poor data fit, the inversion result is not considered reliable and further inversion studies should be carried out.

c) Assess the vertical section through well(s) — can a clear correlation to the well results be seen in the vertical section? This is typically evaluated by cordendering of the well logs and the CSEM inversion result and considering resistivity anomalies and depth placement.

d) Assess average resistivity through the target interval, and use histogram-based anomaly detection. A suitable depth interval is used to extract the resistivity map from a 3D vertical resistivity volume, and lateral bounds on high-resistive anomalies are determined by the distribution of anomalous versus background values in the map. (Figure 7, bottom left).

e) Assess how the results are likely to increase or decrease probability of success and volumes predrilling.

It is important to note that these steps do not describe the complete workflow used for the integrated interpretation — this assessment is only the groundwork required to do an integrated interpretation. The detailed workflow for integrated interpretation is not discussed here.

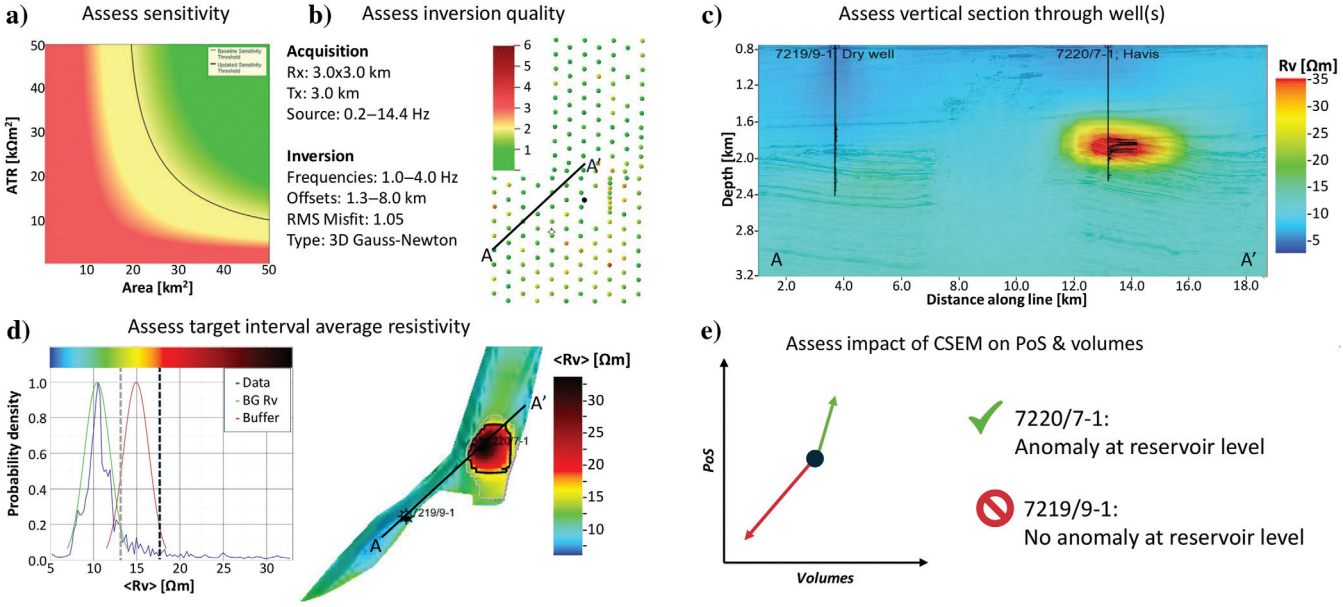

Figure 7. Workflow used for integrated interpretation evaluation of CSEM. This approach takes the sensitivity to volumes into account and will not consider targets below the sensitivity threshold as false negatives. The main text explains the steps: (a) Assess the sensitivity, (b) assess the inversion quality, (c) assess the vertical section with the well, (d) assess the target interval average resistivity, and (e) assess the impact of CSEM on the PoS and volumes.

DOI:10.1190/INT-2019-0307.1

True negatives

The true-negative case is obviously the easiest case to assess. When the well encountered no hydrocarbons and CSEM indicated no hydrocarbons, this really cannot be quantified much further. Although the true-negative case is not something an explorer wants to encounter, it is nevertheless extremely powerful and can have a very large economic impact. Knowing when to walk away is in many cases just as important as finding something worth drilling. These correct identifications of true negatives have the potential to significantly enhance the value of a drilling campaign, as we will show later in the discussion of creaming curves.

False negatives

Due to CSEM sensitivity limitations, the absence of a clear CSEM anomaly does not mean that there will be no volumes to discover at a potential target level, but we may quantify an upper limit of what the exploration well is likely to encounter. This limit is a function of multiple factors, like sensitivity to target and reservoir properties, survey grid resolution, equipment used, and so forth. All these factors can however be accounted for in sensitivity studies and scenario testing. To illustrate this, let us revisit the Filicudi 2017 discovery (Figure 8). The target scenario tests based on CSEM data indicated that no more than 100 MMboe was likely. Postdrill, the operator reduced the estimates from the anticipated 258 MMboe to between 35-100 MMboe, which later was further reduced to 23 MMboe (Rystad Energy, 2018). This overestimation of resources in place is systematic, as discussed in the NPD 2018 resource report (NPD, 2018). The identification of upper volume limits using CSEM can be a powerful correction to mitigate such bias in resource estimation.

The overestimation of resources is reflected generally in the results for the entire Norwegian sample when taking the sensitivity to the volumes discovered into account. We see that there is a distinct lack of commercial discoveries where we have CSEM negatives (Figure 9), whereas all major discoveries are associated with CSEM anomalies. We also see that CSEM failed to detect volumes likely to be produced in a few cases. However, these failures represent cases of minor volumes that can be tied into larger discoveries in an area where infrastructure is already in place. It thus seems clear that the likelihood of discovering commercial volumes of hydrocarbons, when drilling on a CSEM negative with high sensitivity to the assumed volumes in place, is very small.

True positives

We will now look closer into what we can achieve when integrating CSEM results with other geophysical data using a rock-physics framework. As demonstrated by Fanavoll et al. (2014) on the subsequently drilled Pingvin prospect, CSEM can be used to predict the volumes in place and the column height predrilling. Based on 2013 vintage inversion results and scenario testing (see Figure 10), they estimate the mean recoverable resources to be 75 MMboe and the corresponding mean net pay to be 18 m predrilling, thus decreasing the likely volumes discovered while simultaneously increasing the probability of success. The predictions were indeed

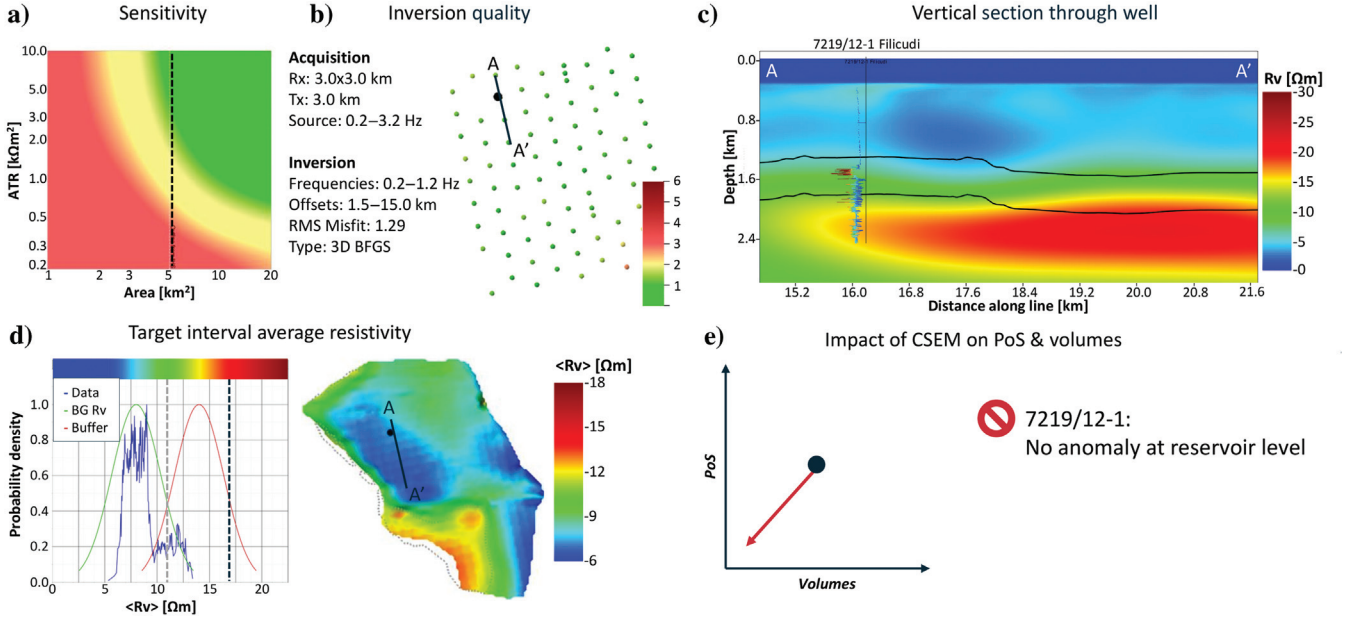

Figure 8. Integrated evaluation for Filicudi based on the legacy 3D BFGS results. The discovery was made in the Early Jurassic Tubåen Formation, around 1500–1700 m TVD. No robust anomaly is identified at the well location, which is what we expect from the sensitivity analysis and the reported discovered volumes, which indicate a low ATR in the reservoir. With respect to what we are supposed to detect, Filicudi is now no longer a false negative.

in line with the published well results, which proved a 15 m gas column and estimated recoverable volumes to be in the range of 30–120 MMboe.

Next, we analyze the true-positive case at the Gemini North prospect. Prior to drilling, this area was surveyed using high-resolution 3D CSEM. The spatial resolution and sensitivity achieved for the shallow resistor were unprecedented, and the survey results were described by Granli et al. (2018). The new data enable quantitative interpretation of a detailed spatial model. This was not possible on the smooth results achieved from previous survey data using a coarse 3 km spaced acquisition grid, as shown in Figure 5a and 5b. We compute ATR by numerical evaluation of an integral of the vertical resistivity contrast over the target depth level. ATR is a quantity that captures the thickness-resistivity ambiguity of CSEM responses and provides a natural upscaling (Granli et al., 2018). The discrepancy in ATR mapped in the two inversion results reflects the quantitative uncertainty of the data sets, which was reduced substantially in the high-resolution data set due to improved sensitivity.

A well prediction was made by integrating CSEM with seismic structure and an electrical rock-physics model calibrated to nearby Wisting petrophysical well interpretations (Morten et al., 2019). The map in Figure 11 (left) shows the predicted column variation across the reservoir. At the well position, the predicted column of 13 m was very close to the well outcome for the corresponding high-resistive reservoir type (Figure 11 right). The different wells at the Wisting discovery have encountered significant variations in the resistivity and rock parameters, which may allow us to discriminate between different reservoir qualities. The corresponding rock-physics models can be tested with the methodology described here to support assumptions on reservoir type at the prospect. Using such methodology, we can build confidence in the interpretation of a resistor and integrate with geologic models.

False positives

The final category are the false positive cases in which a resistor has been mapped, and then confirmed by the well, but the well was not a hydrocarbon discovery. We will analyze two recent cases, namely, the wells at the Koigen (7317/9-1) and Pointer/Setter (7121/1-2 S) prospects.

The Koigen case was described by Morten et al. (2019), and we only review the main findings. The prospect is situated in the Stappen High area of the Barents Sea, and a large, high-resistivity area was mapped at the target interval from coarse-grid 3D CSEM data acquired in 2012. The well encountered multiple sandstone layers with poor to no reservoir quality, and the well is classified as dry. The sandstone layers represent tight and highly resistive lithology, which is believed to be the origin of the CSEM mapped resistor. The risk of such antimodel can be assessed using quantitative analysis of the 3D CSEM inversion results. By constructing electrical rock-physics models, it is possible to relate the ATR to the thickness of the resistive rock. The resistive rock could be considered as either representing a fluid scenario or resistive lithology, for example, cemented sandstone. Well data or analogues are

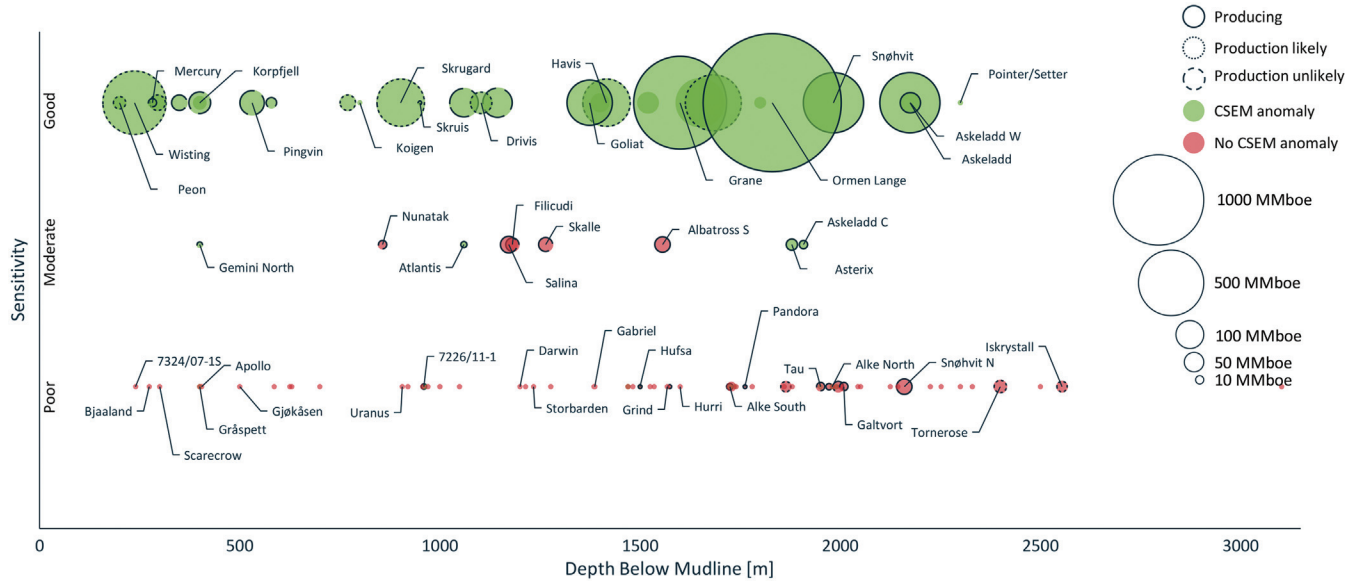

Figure 9. Sensitivity versus depth below mudline (m). The size of the bubble indicates the volumes discovered; dry wells are represented by a dot. Sensitivity to the volumes is grouped into three distinct categories: poor, moderate, and good, where we expect to always be able to image a target with good sensitivity and never targets with poor sensitivity. For a target with moderate sensitivity, we will sometimes be able to image the target and sometimes not, depending on, among other factors, the complexity of the geology in the area and the density of the acquisition grid. Green indicates CSEM anomaly associated with the discovery, and red indicates the absence of a CSEM anomaly. High-impact and recent wells are highlighted. Volumes are sourced from NPD and from public information.

typically required to calibrate such models. For Koigen, well 7318/12-2 is relevant, and it encountered a tight and high-resistivity reservoir. The mean models for the ATR relationship used in the quantitative analysis show that at the Koigen well position, the ATR corresponds to 81 m good-quality HC-saturated reservoir or 109 m cemented sandstone. However, these figures are associated with error margins due to the assumption of the rock properties. Nevertheless, it would be possible to compare this to the seismic mapped reservoir layers thickness predrilling. Indeed, the well encountered total tight reservoir thickness close to 110 m.

Let us now consider the Pointer/Setter prospects tested by exploration drilling in 2019. Figure 12 shows a vertical section of the resistor imaged by 3D CSEM and the relevant stratigraphic layers. The Pointer and Setter prospects are located 20 km north of the Snøhvit gas field in the Barents Sea. In the analysis, we will consider Snøhvit as an analogue for Pointer/Setter and use exploration well data from Snøhvit for calibration of the rock-physics model. Figure 13

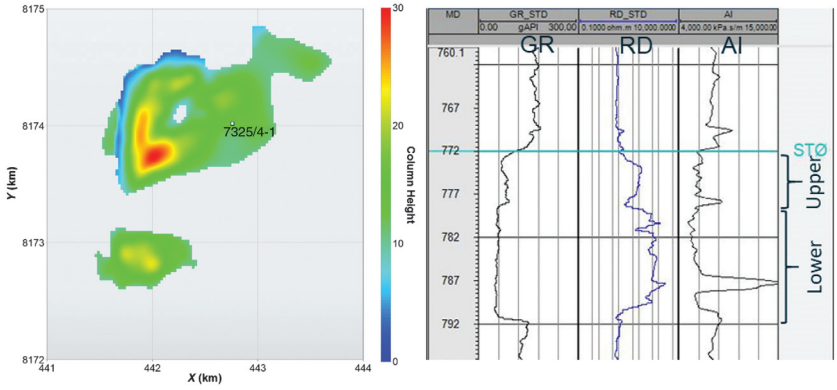

Figure 11. Left: Prediction of the HC-saturated reservoir column at Gemini North using the ATR map from high-resolution 3D CSEM and an electrical rock-physics model calibrated to the Stø reservoir encountered in well 7324/8-2 (Hanssen). At the Gemini North well position, the column height is 13 m. Right: the Gemini North well outcome; GR, gamma ray; RD, resistivity deep; and AI, acoustic impedance. The good-quality HC-saturated Stø reservoir in the lower interval is approximately 13.5 m thick.

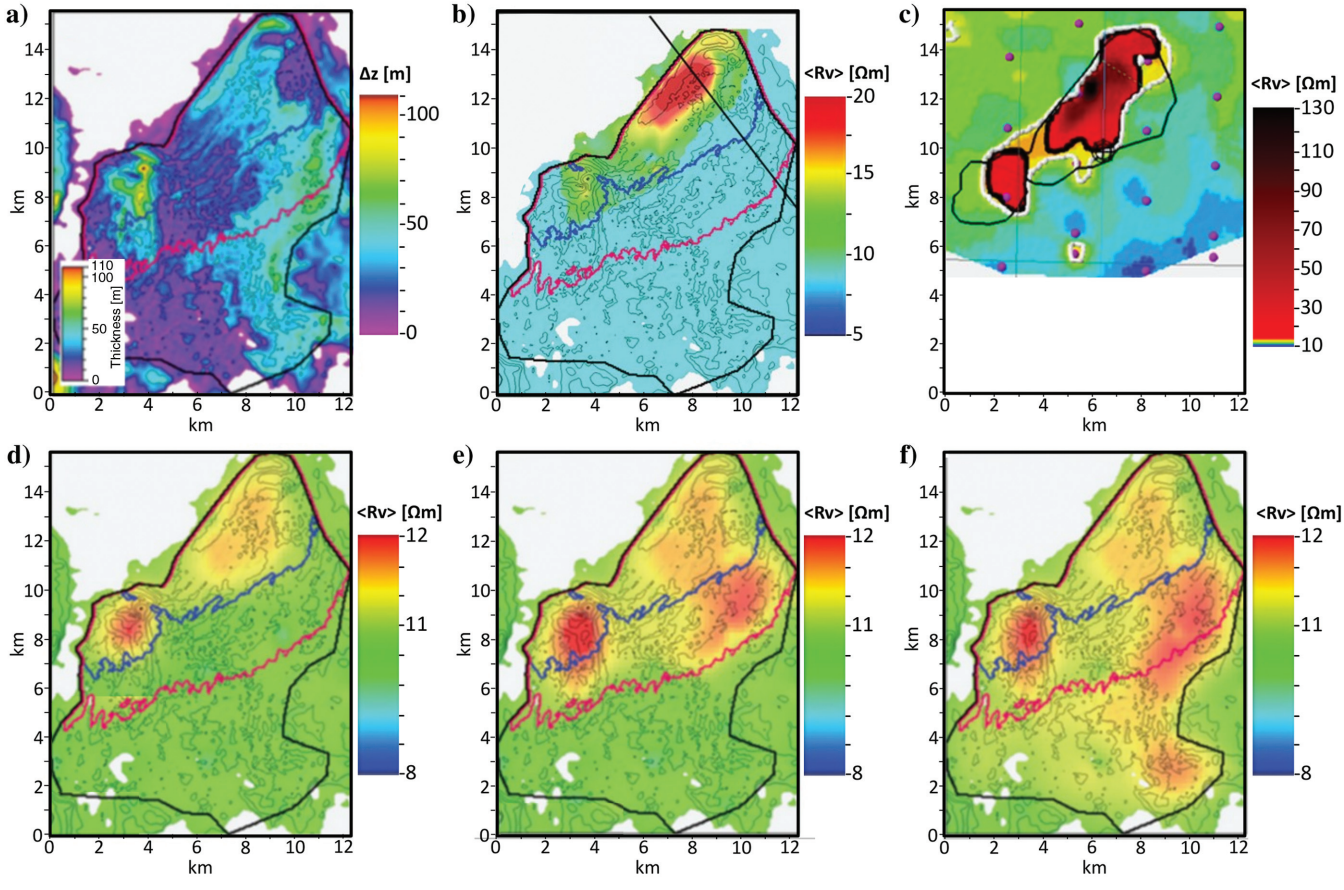

Figure 10. (a) Isochore along with (b) the average resistivity for legacy 3D BFGS and (c) a recent 3D Gauss-Newton inversion of the Pingvin data set. Bottom row: Average resistivity from the legacy 3D BFGS scenario test for the (d) low, (e) mean, and (f) high cases for the Pingvin prospect indicate that the low case is the most likely based on CSEM results. Note that, despite the increased resistivity recovery from the 3D Gauss-Newton inversion, we still do not see an anomalous response outside the low case scenario outline. The purple dots in (c) represent the receiver positions.

DOI:10.1190/INT-2019-0307.1

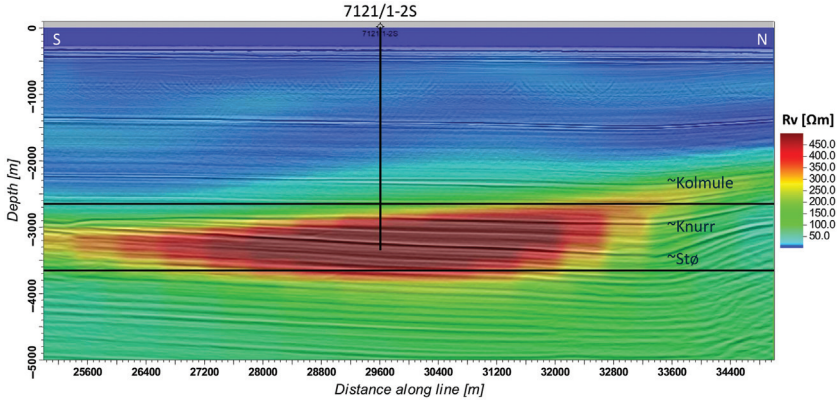

Figure 12. Seismic section through Pointer/Setter corendered with CSEM. The thickness of the Knurr wedge is around 300 m at the thickest part. Note that the CSEM is in depth, whereas the seismic is in time and is stretched to fit around the Knurr level. Due to the high velocities in the area, this pseudo-depth conversion is highly uncertain and the fit between CSEM and seismic is rather poor.

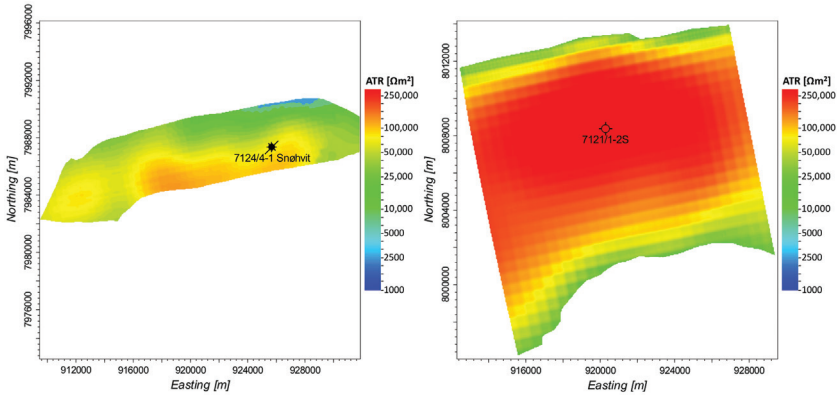

Figure 13. ATR map for the Snøhvit discovery (left) and the Pointer/Setter prospect (right).

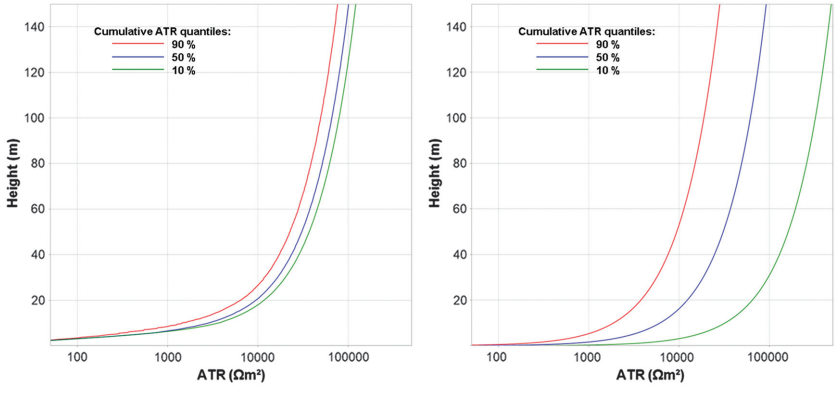

Figure 14. Rock-physics models relating height and ATR for resistive rocks. The ATR distributions from Monte Carlo simulations are shown in terms of cumulative probability quantiles; that is, the 10% quantile means that only 10% of the models exceed this ATR value. Left: Fluid scenario using Archie's equation and normally distributed NTG and shale layer thickness. The NTG distribution has a mean of 80% and a standard deviation of 15%, the shale layer thickness has a mean of 5 m and a standard deviation of 3 m. The parameters are calibrated to well results from Snøhvit. Right: Tight reservoir scenario (SW = 100%) with porosity normally distributed with a mean of 3% and a standard deviation of 1.5%.

compares the ATR maps over the Snøhvit field (left) and the Pointer/Setter prospects (right) as imaged by 3D CSEM inversion. The figures show that the ATR is significantly larger at Pointer/Setter than at Snøhvit. At the indicated well positions, the ratio is approximately 6. This is already an indication that the resistor at Pointer/Setter may be of another origin than the HC reservoir at Snøhvit because the reservoir properties at Snøhvit are expected to be superior to those at Pointer/Setter, but quantitative interpretation can further substantiate this.

The evaluation report for Snøhvit exploration well 7121/4-1 gives detailed information about the porosity, water saturation, net-to-gross, and shale content for the Jurassic reservoir. We use this information together with the well logs to calibrate the electrical rock physics. In Figure 14 (left), we show the resulting height-ATR relationship for this model where we incorporated a statistical representation of the shale lamination. The P50 prediction for the gross HC-saturated reservoir column at the well position agrees very well with the well outcome using the rock-physics model and the mapped ATR.

We now transform the ATR map over Pointer/Setter in Figure 13 (right) to the map of gross HC-saturated reservoir thickness shown in Figure 15 (left). This analysis shows that given the assumption of similar reservoir parameters as Snøhvit, we would need a column height peaking above 600 m to explain the prospect ATR that is mapped by CSEM. This holds for all the ATR quantile distributions shown in Figure 14 (left), and the map in Figure 15 (left) shows the result for the P10 relation (i.e., the relationship corresponding to the statistical quantile where only 10% of the models exceed the simulated ATR from reservoir property distributions). Such a column height is not supported by the seismic data, as seen in Figure 12. Let us instead consider the cemented sandstone reservoir as a resistor antimodel. In Figure 14 (right), we show the thickness-ATR relationship for such a rock-physics model in which we incorporated a statistical model for the porosity distribution. In contrast to the fluid case, we see that a much higher ATR is within range for this scenario. When we apply

DOI:10.1190/INT-2019-0307.1

the P10 percentile relation to map the ATR into tight reservoir thickness, we achieve the map shown in Figure 15 (right). At the well position, the thickness prediction 140 m is close to the well outcome. The well encountered approximately 130 m of tight reservoir with low reservoir quality. This prediction is also in good agreement with the observations from the seismic. Note that our modeled P50 (i.e., the relationship corresponding to the statistical quantile in which only 50% of the models exceed the simulated ATR from the reservoir property distributions) cemented reservoir prediction results in a thickness that is larger than the feasible range from seismic, indicating porosity properties in the lower value range modeled.

Summarizing the quantitative interpretation, we have shown how such an analysis could substantiate downgrading the chance of success for the Koigen and Pointer/Setter wells predrilling if we had performed such a study prior to spud. However, the extent of update to probability of success is different for these two cases. For Pointer/Setter, the Snøhvit analogue scenario is improbable, whereas the antimodel scenario is supported by CSEM. For Koigen, we are prompted to balance the fluid and antimodel scenario in risking. The workflow exemplified here shows how cases in the false-positive category can be worked to provide valuable information for further evaluation in exploration.

Discussion

We have presented statistics from a large sample of exploration wells and correlated to CSEM results achieved without integrated interpretation, demonstrating a match between CSEM and well results of 79%. This figure is also in line with findings from other authors, such as Price et al. (2019), who cite a success ratio of 80% even for pessimistic assessments of the qualitative correlation between the well results and CSEM.

If the results from this study are used in a Bayesian framework, we see that a CSEM positive will increase the probability of success drastically, whereas the absence of a CSEM anomaly is indicative of a minor discovery or a technical success. In Figure 16, we visualize how the input information from CSEM can affect the probability of success (PoS). In this example, if the CSEM prospect evaluation is negative, a prior PoS is reduced from 34% to 13%. In case of a positive CSEM evaluation, the prospect PoS is increased to 81%. This strong polarization of the PoS by integrating CSEM information can have a large effect on a prospect portfolio. Further details for this type of PoS update are discussed in Barker and Baltar (2015).

In summary, we have showcased workflows that demonstrate that integrated interpretation can improve on an already high success ratio, especially with respect to distinguishing between technical success and commercial success. The potential impact of integrating CSEM and using such workflows is clearly identified in Figure 17, where we compare the creaming curve (Rose, 2001) in the Barents Sea based on the database discussed in this study. In Figure 17 (top), we show the actual creaming curve, which is compared to a hypothetical creaming curve (bottom) where we consider the scenario in which the cases with a CSEM-positive outcome are the exploration wells drilled first. If we look at the performance after 10 wells, we see that in the CSEM-driven scenario, we are already outperforming the classic scenario by 150 MMboe.

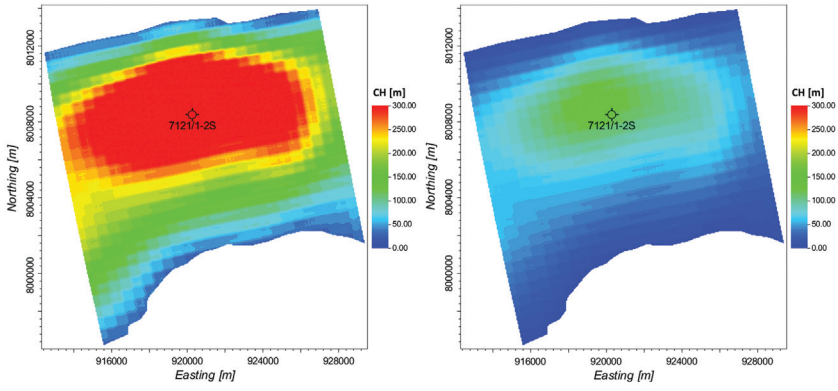

Figure 15. Left: Gross HC-saturated column height (CH) for the Pointer-Setter prospect derived from CSEM assuming the rock-physics model for the Snøhvit reservoir. At the well position, the column exceeds 300 m. Right: Resistive tight reservoir thickness for the Pointer/Setter prospect derived from CSEM assuming a cemented sandstone case. The thickness at the well position is 140 m.

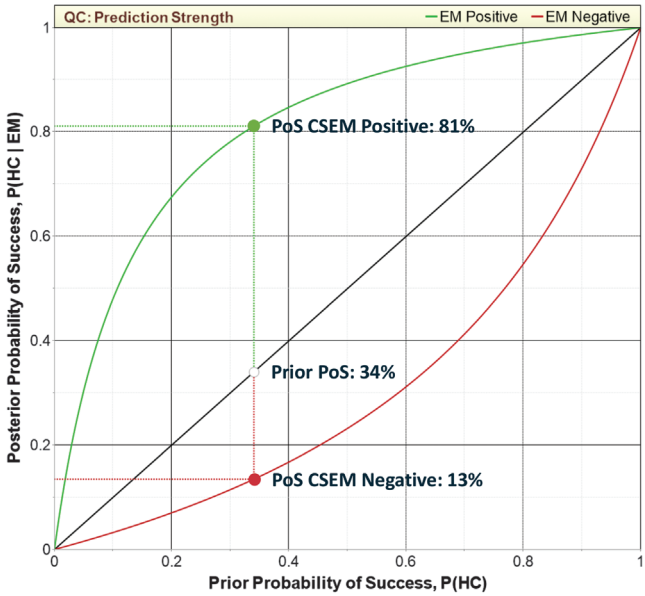

Figure 16. Update to PoS by integrating CSEM into the prospect evaluation.

DOI:10.1190/INT-2019-0307.1

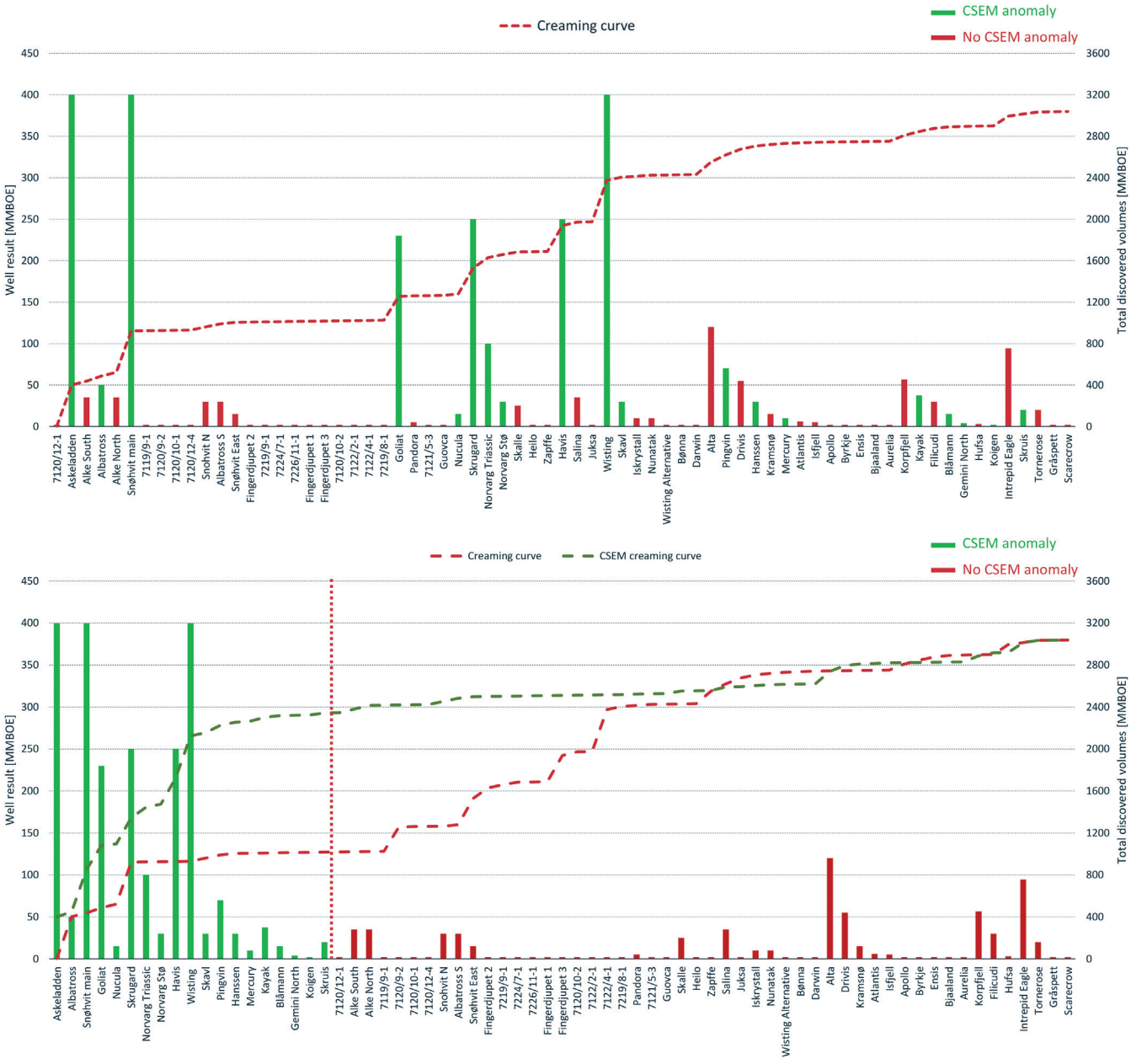

Figure 17. Barents Sea actual exploration history and creaming curve where multiclient CSEM data are available (top) versus a hypothetical Barents Sea exploration history and creaming curve if CSEM positives had been drilled first.

Conclusion

We have assessed a large database of 3D CSEM data and correlated the results to exploration drilling outcomes. The prediction strength calculated as the correct prediction of true-positive or true-negative cases is 79%. This shows that incorporating 3D CSEM information has the potential to substantially enhance exploration success because discovery rates are typically much lower. Our comparison of the actual and a hypothetical creaming curve in which 3D CSEM is used for prospect ranking further emphasizes the commercial potential of the multiphysics workflow. We therefore conclude that the integration of 3D CSEM with seismic can significantly improve exploration performance.

Our results also show how quantitative interpretation can supplement the interpretation from seismic. In some scenarios, we can derive information about the reservoir properties for more detailed volume assessments; in other cases, this approach makes it possible to determine the risk of antimodels to correctly interpret false positives as such — thus turning false positives into true negatives.

Acknowledgments

The authors thank EMGS for permission to show the CSEM results in this paper.

Data and materials availability

Data associated with this research are confidential and cannot be released.

References

Barker, N., and D. Baltar, 2015, Prospectivity evaluation with 3D CSEM: First Break, **33**, 55–62.

Barker, N., and D. Baltar, 2016, CSEM anomaly identification; First Break, **34**, 47–50.

Fanavoll, S., P. T. Gabrielsen, and S. Ellingsrud, 2014, CSEM as a tool for better exploration decisions: Case studies from the Barents Sea, Norwegian Continental Shelf: Interpretation, **2**, no. 3, SH55–SH66, doi: 10.1190/INT-2013-0171.1.

Granli, J. R., D. Daudina, S. C. Robertson, J. P. Morten, P. T. Gabrielsen, and B. Sigvathsen, 2018, High resolution 3D CSEM for reservoir characterization: 88th Annual International Meeting, SEG, Expanded Abstracts, doi: 10.1190/segam2018-2995351.1.

Mittet, R., and J. P. Morten, 2012, Detection and imaging sensitivity of the marine CSEM method: Geophysics, **77**, no. 6, E411–E425, doi: 10.1190/geo2012-0016.1.

Mittet, R., and J. P. Morten, 2013, The marine controlled-source electromagnetic method in shallow water: Geophysics, **78**, no. 2, E67–E77, doi: 10.1190/geo2012-0112.1.

Morten, J. P., J. O. Jenssen, E. A. Nerland, P. T. Gabrielsen, and J. R. Granli, 2019, CSEM quantitative interpretation for reservoir property estimation and anti-model evaluation: 89th Annual International Meeting, SEG, Expanded Abstracts1009–1013, doi: 10.1190/segam2019-3214693.1.

Nguyen, A. K., P. Hanssen, R. Mittet, H. R. Jensen, L. T. T. Fogelin, M. Skarø, M. Rosenquist, and P. van der Sman, 2017, The next generation electromagnetic acquisition system: 79th Annual International Conference and Exhibition, EAGE, Extended Abstracts, doi: 10.3997/2214-4609.201700567.

Nguyen, A. K., J. I. Nordskag, T. Wiik, A.K. Bjørke, L. Boman, O. M. Pedersen, J. Ribaudo, and R. Mittet, 2016, Comparing large-scale 3D Gauss–Newton and BFGS CSEM inversions: 86th Annual International Meeting, SEG, Expanded Abstracts, doi: 10.1190/segam2016-13858633.1.

Norwegian Petroleum Directorate, 2018, Resource Report 2018 — Exploration, online report, https://www.npd.no/en/facts/publications/reports2/resource-report/resource-report-2018/.

Price, A., C. Twarz, and P. T. Gabrielsen, 2019, Building confidence in CSEM for Exploration — Benchmarking: 89th Annual International Meeting, SEG, Expanded Abstracts doi: 10.1190/segam2019-3214720.1.

Rose, P. R., 2001, Risk analysis and management of petroleum exploration ventures: AAPG Methods.

Rystad Energy, 2018, NCS E&P Newsletter, February 2018.

Westwood Global Energy Group, 2018, Advances in exploration eechnology and geosciences — Past and future on the NCS, report 2018, https://www.westwoodenergy.com/news/westwood-insight/exploration-technology-and-exploration-performance-offshore-norway.

Ziolkowski, A., and E. Slob, 2019, Introduction to controlled-source electromagnetic methods — Detecting subsurface fluids: Cambridge University Press.

Lodve Berre received an M.Sc. from the Norwegian University of Science and Technology (NTNU) in environmental physics in 2003. He is currently I&I solutions manager at EMGS and has 14 years of experience in technical sales and the inversion and integration, processing, and acquisition of CSEM data. His research interests include improved imaging of CSEM data and integration of geophysical data for improved reservoir characterization. He is an active member of EAGE.

Jan Petter Morten received a Ph.D. from NTNU in physics in 2008. He is currently R&D manager at EMGS and has 12 years of experience in developing tools for marine EM data processing, modeling, and inversion with application to exploration and reservoir characterization. His research interests include integration of geophysical data for improved reservoir characterization, time-lapse applications of CSEM, full-waveform inversion, and 3D modeling. He is an active member SEG and EAGE.

Graeme Baillie received science degrees from New Zealand and Western Australia with postgraduate qualifications in geophysics. Graeme started his career as a geophysicist with Santos in Australia and has worked in Africa, the Middle East, and Asia Pacific. He joined EMGS in June 2016 as exploration advisor for the Asia-Pacific region. Prior to that, he worked for Lundin Petroleum from 2006 to 2016 as new ventures advisor in Singapore and exploration manager for Lundin Malaysia.

Elias-Andre Nerland received an M.Sc. from NTNU in geophysics and petroleum technology in 2003. He is currently an interpretation advisor at EMGS and has 9 years of experience working with electromagnetic data and integrating them into the exploration workflow. Prior to EMGS, he worked at Norsk Hydro from 2003 and at Statoil from 2007 doing seismic interpretation, well planning, lithology prediction from seismic inversion, and seismic monitoring.